Progress In Electromagnetics Research, Vol. 130, 389–409, 2012

A NOVEL COMPACT SPLIT RING SLOTTED ELECTROMAGNETIC BANDGAP STRUCTURE FOR MICROSTRIP PATCH ANTENNA PERFORMANCE ENHANCEMENT

M. S. Alam[1, 2], M. T. Islam[2, *], and N. Misran[1, 2]

[1]Department of Electrical, Electronic and Systems Engineering, Universiti Kebangsaan Malaysia, Bangi, Selangor 43600, Malaysia

[2]Institute of Space Science (ANGKASA), Universiti Kebangsaan Malaysia, Bangi, Selangor 43600, Malaysia

Abstract—A novel design of an electromagnetic bandgap (EBG) structure based on the uniplanar compact EBG (UCEBG) concept is proposed in this paper. The structure is realized by inserting split-ring slots inside two reversely connected rectangular patches, which is known as a split-ring slotted electromagnetic bandgap (SRS-EBG) structure. The bandgap properties of the EBG structure are examined by the suspended microstrip line and finite element methods (FEM). The achieved bandgaps have widths of 4.3 (59.31%) and 5.16 GHz (38.88%), which are centered at 7 and 13 GHz, respectively. The SRS-EBG is applied to enhance the performance of a single-element microstrip patch antenna (at 7 GHz) and a two-element array (at 13 GHz) configuration. A wider bandwidth is obtained with a better reflection coefficient level for the single element antenna; a reduction in mutual coupling of more than 20.57 dB is obtained for the array design. In both cases, the gain and radiation characteristics are improved. The results are verified by measuring the fabricated lab prototype, and a comparison with the computed results showed good agreement.

1. INTRODUCTION

Immense growth and advancement in wireless communication technology increases the demand for highly efficient compact devices. It is a challenge to be compatible with a wide range of small-scale applications while maintaining good performance. In the RF

Received 7 June 2012, Accepted 1 August 2012, Scheduled 20 August 2012

* Corresponding author: Mohammad Tariqul Islam (titareq@yahoo.com).

and microwave research arena, microstrip patch antennas are a smart solution for compact and cost effective wireless communication systems. Features such as light weight, low volume, low profile, low fabrication cost, robustness, ease of mounting on the host surface and integration with printed circuits led their use in a wide range of applications. However, compared to non-printed antennas, these types of antennas suffer from a number of drawbacks, such as narrow bandwidth, low gain, poor radiation performance due to excitation of surface waves, etc. [1–4]. The application of a thick, low permittivity substrate, a stacked configuration or a ferrite composition improves bandwidth while increasing the volumetric size and cost. Another way to improve bandwidth is to use non-contacting feeding techniques, which are associated with fabrication difficulty [5, 6]. Meanwhile, the array configurations of patch antenna are usually designed for applications in which high gain antennas are required. However, the excitation of surface waves introduces mutual coupling between the adjacent elements of an array; this coupling effect become very significant at higher substrate permittivities, thicknesses and operating frequencies. The coupling between elements can cause scan blindness of an array and form blind spots. By enlarging the gap between elements, mutual coupling can be reduced, but this enlargement introduces undesirable grating lobes [7–9]. Considering these factors and the advantages of microstrip patch antennas, the incorporation of electromagnetic bandgap (EBG) structures is an attractive research idea in the antenna community. The term 'EBG' is modeled after photonic bandgap (PBG) structures in optics because of their analogous properties of wave propagation and restriction at certain frequency ranges, which is known as a bandgap [10–12].

EBG structures are a significant breakthrough for enhancing microstrip antennas performance. They have been used as a component of resonant cavities, filters, couplers, dividers, amplifiers, etc. [13–15]. EBG structures are usually periodic arrangements of metallic or dielectric elements that exhibit bandstop or bandgap characteristics. They are sensitive to the permittivity and thickness of the substrate and, most importantly, to the EBG geometry. The main properties of EBG structures are the ability to guide and control electromagnetic wave propagation and surface wave suppression within the bandgap range, which improves antenna performance by reducing back radiation, and mutual coupling, as well as cross polarization [16–20]. Most early research focused on three-dimensional EBG structures that were structurally complicated, heavy and difficult to integrate with microwave circuits. To avoid complexity, planar EBGs (mushroom shape, fork-like shape, spiral

shape, etc.) that realized through grounding vias have been studied extensively [10, 21, 22]. Because the period of an EBG structure must be a half-wavelength at the bandgap frequency, accommodating their physical size becomes problematic when integrated with printed circuits and antennas. Although these conventional EBG structures are widely used to suppress unwanted surface waves, the cell size should be considered for practical applications. Additionally, the presence of a grounded via connection is associated with design and fabrication complexities, which led the researchers to investigate uniplanar shaped EBG. These structures require no grounding via and can easily be fabricated on standard PCB materials. Both theoretical and experimental advancement have driven the rapid development of EBG technology, with emphasis on designing compact and uniplanar shaped EBG structures. Uniplanar Compact EBG (UC-EBG) structures are designed to realize a high impedance surface that arises from a distributed 2D periodic LC network [23]. The LC characteristics of the UC-EBG structures are provided by the metallic patches and interconnecting thin bridges, which will be detailed in the design section.

Many planar EBG structures have been proposed and applied to improve antenna performance in diverse ways [24–31]. Leaf shaped bowtie patch antennas incorporated with an $100 \times 100\,\text{mm}^2$ EBG reflector exhibit improved radiation patterns, gain and directivity [30]. Different patch sizes have been examined within the 7–10 GHz range and a low-profile, wideband, unidirectional antenna has been realized by using the EBG. In [31], the integration of an array of UC-EBG with an antenna array operating at 12.2 GHz reduced the mutual coupling to -39 dB. The configuration, which was built on a high permittivity substrate, reduced coupling by 20.5 dB. The fork-like planar EBG proposed in [21] demonstrated 6.51 dB better reduction of mutual coupling than a conventional design, which only reduced coupling by 2.02 dB with an unperturbed metal patch. A 3×7 mushroom-EBG matrix inserted between a two element microstrip patch antenna array reduced coupling by 10 dB at 5.8 GHz [8]. The UC-EBG structure examined in [7] lowered the coupling level to -27 dB from -14 dB, and 0.7 dB of gain and a 31% bandwidth increment have been observed for a dipole antenna array. However because compactness is so desirable, there is still reason to find a more compact UC-EBG that would improve antenna performance and be compatible with more applications.

In this paper, we propose a novel split-ring slotted uniplanar EBG (SRS-EBG) configuration with dual wide bandgaps and compact size. The bandgap of the vialess SRS-EBG is studied and analyzed by

the suspended microstrip line method, and the design is validated by applying it to a single element microstrip antenna and a two element microstrip patch antenna array. The EBG configuration is applied as an artificial ground to a microstrip patch antenna that operates within the first bandgap. Coupling reduction is investigated by incorporating the SRS-EBG in between a microstrip antenna array for the second bandgap. Significant improvements in bandwidth, gain, and radiation characteristics and a reduction of the mutual coupling level are observed in both cases. Regardless of size, inclusion of the SRS split-ring slot in the EBG improves the effectiveness of the design.

2. DESIGN OF A NOVEL SPLIT RING SLOTTED PLANAR EBG (SRS-EBG)

The design of a compact uniplanar configuration with a high impedance surface is a significant challenge. The absence of a ground-connecting via, as used in other designs, makes the challenge significant but not impossible. The EBG configuration must be designed carefully considering the frequency sensitivity of the periodic structure's surface impedance. The high impedance characteristic arises from the distributed LC characteristics of a network designed for the specific frequency range of interest. The electromagnetic characteristics of EBG structures can be demonstrated by using inductors and capacitors. The equivalent LC network acts as a two-dimensional electric filter within the frequency range where the structure surface exhibits high impedance. Within the range of the surface block, the surface waves propagate in the substrate material. Therefore, consideration of these two factors is important in determining the bandgap of an EBG structure.

No specific formula exists to express the impedance nature of an EBG realized with an irregular shape unit cell. However, the inductance and capacitance of a surface configured with a square EBG unit cell with patch size ($W \times W$) can be described by the following equations [10]:

$$L = \mu_r \mu_0 h \tag{1}$$

$$C = \varepsilon_0 (\varepsilon_r + 1) \frac{(W+g)}{\pi} \ln \left\{ \cos \frac{\pi g}{2(W+g)} \right\} \tag{2}$$

In these equations, ε_o and μ_o are the permittivity and permeability of free space, respectively; ε_r and μ_r are the relative permittivity and relative permeability, respectively; g is the gap width between adjacent cells; W is the patch width; and h is the thickness of the substrate.

By using the calculated values of L and C from (1) and (2), the center frequency of the EBG structure can be predicted by (3), and the width of the bandgap can be predicted by (4).

$$f = \frac{1}{2\pi\sqrt{LC}} \tag{3}$$

$$BW = \frac{1}{\eta}\sqrt{L/C} \tag{4}$$

Each of the distributed circuit elements can be tuned to operate at the desired frequency bands by varying their width and length. The geometry of the proposed split-ring slotted planar EBG (SRS-EBG) is illustrated in Figure 1. To achieve a high-impedance surface, the initial rectangular patch array design is gradually modified to that shown in the following figures.

The initial rectangular unit cell is divided in half by an interleaved gap in which the two halves are interlinked by two other thin microstrip lines. Then, two split-ring slots (SRSs) are introduced into each of the halves, which increase the surface inductance. Two inner patches surrounded by outer interconnected rings are realized without increasing the cell size, which causes some additional capacitances to form between the outer ring and the inner patch. A cross shaped slot is added to the center of the unit cell, which adds further gap capacitances. The overall size of the EBG remains unchanged. Unlike

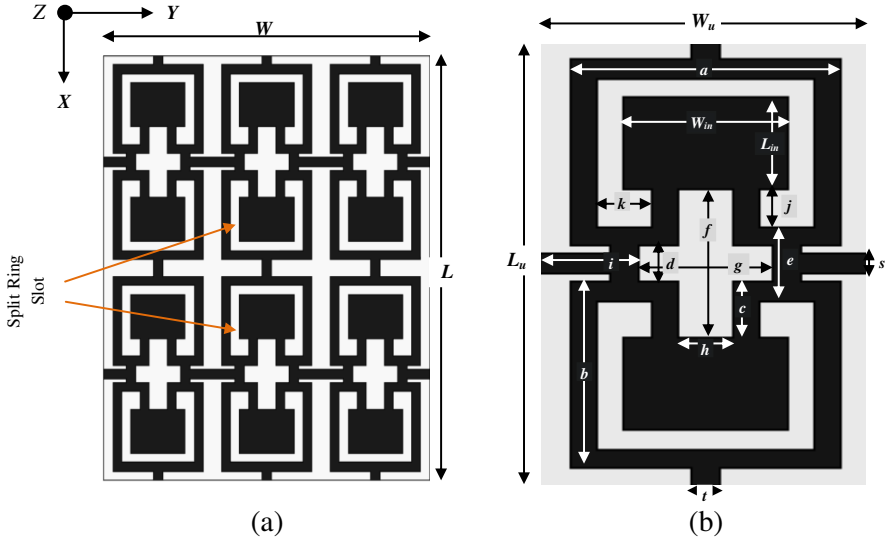

Figure 1. Proposed planar SRS-EBG configuration: (a) 2×3 array of EBG; (b) Unit cell geometry.

other planar designs, the uniplanar design does not incorporate any type of grounding via. Therefore, all of the inductive and capacitive effects should be produced by the uniplanar EBG surface. To ensure this and to maximize the bandgap, the EBG unit cells are interconnected to adjacent cells by four thin microstrip lines. This interconnection increases the total L and C of the EBG surface. Because the effect of the structure is integral, all possible parameter variations must be considered. In the following sections, bandgap characterization of the proposed SRS-EBG is performed by parametric studies.

3. PERFORMANCE ANALYSIS OF THE UNIPLANAR SRS-EBG

To analyze the bandgap characteristics of the proposed SRSs EBG structure, the suspended microstrip line method [32] is used, as shown in Figure 2. In contrast to the classical microstrip and monopole method, the suspended microstrip structure shows strong coupling nature and eliminates the effect of parasitic propagation, which helps to achieve the desired characteristics [20]. The EBG structure is built on a commonly available, inexpensive, 1.6 mm thick FR4 substrate with a relative permittivity of 4.6 and a tangent loss of 0.0027. A thin microstrip line of 3 mm with a 50 Ω characteristic impedance is printed on the opposite layer of the dielectric material and soldered with two subminiature A (SMA) connectors on both sides to measure the transmission characteristics. The bandgap properties are computed by varying different design parameters, such as bridge width, inner patch size and unit cell size.

To see the effect of the connecting bridge width on the bandgap, the width is varied along the X-axis (t), the Y axis (s) and both axes (s, t) with all other parameters fixed. As depicted in Figure 3, the bandgap characteristics are affected by varying the bridge width. Combinations

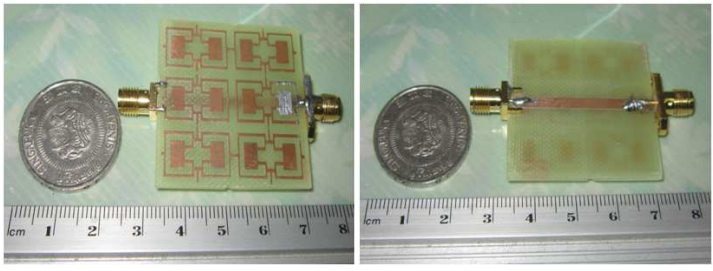

Figure 2. Method of suspended microstrip line to investigate bandgap, front and back view of the fabricated prototype.

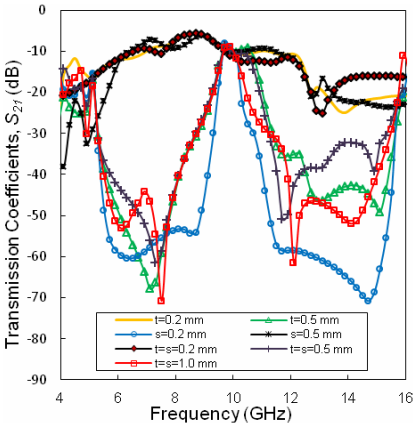

Figure 3. Transmission characteristics with bridge width variation.

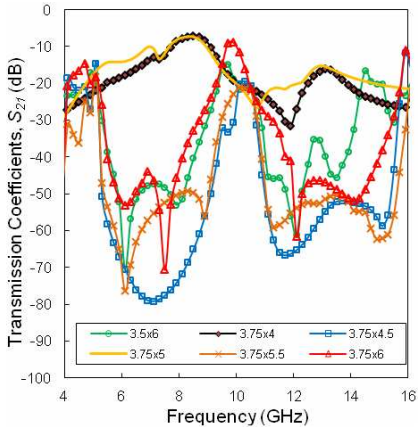

Figure 4. Transmission characteristics with inner patch size variation.

of s and t from 0.2 mm to 1 mm are examined, keeping either one fixed to 1 mm. The minimum transmission coefficient S_{21} (dB) and the center frequency vary, though the bands remain approximately at 7 GHz and 13 GHz. The bandwidth of the first bandgap obtained is 4.45 GHz (5.1–9.55 GHz) for $s = 0.2$ mm, $t = 1$ mm and 4.2 GHz (5.1–9.3 GHz) for other bridge width combinations. In the second bandgap region, for $s = 0.2$ mm, the -20 dB bandgap extends from 10.5 GHz to 15.7 GHz with a bandwidth of 5.2 GHz, with coupling reduction superior to other widths tested. The width combination has significant control over the bandgap and S_{21} dB level; this effect is simultaneous. When the widths are equal to 0.5 mm and 1 mm, the presence of the bandgap is obvious, but $s = 0.2$ mm produces contrary results. A bridge width of $s = 0.5$ mm ($t = 1$ mm, fixed) does not exhibited any blocking band, while $t = 0.5$ mm ($s = 1$ mm, fixed) exhibits a good band with a sharp decrease at 7.1 GHz. A similar phenomenon with a reverse effect from s and t is observed when one of s or t is 0.2 mm and the other is fixed at 1 mm. However, the coupling reduction level (S_{21}) varies from -47 dB to -72 dB for all widths. Thus, proper selection of bridge width combinations is important because the inductances, bandgap and S_{21} (dB) level vary with the connecting bridge width. Analysis is then performed by varying the inner patch size and split-ring width. The transmission results are shown in Figure 4. Because each of the patches is inside a split-ring slot, a gap is maintained between the outer ring and inner patch to provide additional capacitive effects. When the patch size

($W_{in} \times L_{in}$) is varied, the gap width varies accordingly. This variation also caused the bandwidth to change. When W_{in} varies from 3.5 to 3.75, no considerable bandwidth enhancement is observed; however, the L_{in} values affect the bandwidth considerably.

No bandgap with desirable characteristics is obtained with a 4 or 5 mm long inner patch. However, 4.5 mm and 5.5 mm long and 3.75 wide inner patches exhibit a wide bandgap and low transmission level. A first bandgap of 5.2 GHz and second bandgap of 5.1 GHz are achieved with patch dimension of $3.75 \times 4.5\,\text{mm}^2$. Thus, the length of the inner patch is the dominant parameter to obtain two bandgaps in the frequency ranges from 5.1 to 10.3 GHz and 10.7 to 15.8 GHz. The obtained bandwidths are 67.53% and 38.5%, respectively with respect to the center frequencies.

The above parametric studies show two wide bandgaps centered at 7 GHz and 13 GHz with the same EBG structure. Further studies are performed to clarify the dual bandgap mechanism of the proposed design; the results are shown in Figure 5(b). An initial design without any SRS, using only two interconnected rectangular patches, exhibits a bandgap from 13 to 16.9 GHz. When a rectangular gap is created in each of the two halves of a unit cell by removing the middle patch, as shown in Figure 5(a), the bandgap position shifts significantly. The new bandgap range is from 6.9 to 9.3 GHz, with a sharp decrease at 8.2 GHz. Two bandgaps are found at two different positions due to the presence of the patch and the creation of a rectangular gap inside the patch. Thus, a cutting SRS is applied so that a middle patch exists with a gap from the outer ring. The insertion of the SRS creates extra gap capacitances, and the outer rings add additional inductive effects. Therefore, a balanced inductive-capacitive effect is produced by the electromotive force, generating a current that flows through the rings and gaps. The existence of a dual bandgap is identified by the SRS and wider bandgaps are obtained. To obtain deeper and wider stopbands, cross-shaped mid slots are introduced as shown in Figure 5(c). Without the mid slots, neither the first nor the second bandgap is found. It is clearly depicted in the figure that the first bandgap is contributed by the mid slot X, while the second bandgap is caused by the mid slot Y. Therefore, the inserted SRS and the mid slots along X and Y provide the balanced resonance behavior of the proposed SRS-EBG configuration, providing two wider bandgaps and very low level of transmission characteristics.

Figure 5(d) demonstrates a different aspect of the proposed SRS-EBG structure. Because the design creates dual bandgaps, we investigate the effect of the different parameters on the center frequencies of the bandgaps. Although the bandgap characteristic is

an integrated effect of various design parameters, some parameters have a more significant effect than others. Figure 5(d) shows that the connecting link between the outer ring and the middle patch is important to the control of the center frequency. When the middle patches are disconnected from the outer rings, the bandgaps shift to higher frequencies (11 GHz and 15.9 GHz). The transmission levels (S_{21}) are not significant. However, when one middle patch is connected by both links (link 1 and 2 or link 3 and 4), the center frequencies shift to 10.2 GHz and 15.1 GHz. Deeper and wider bandgaps are observed

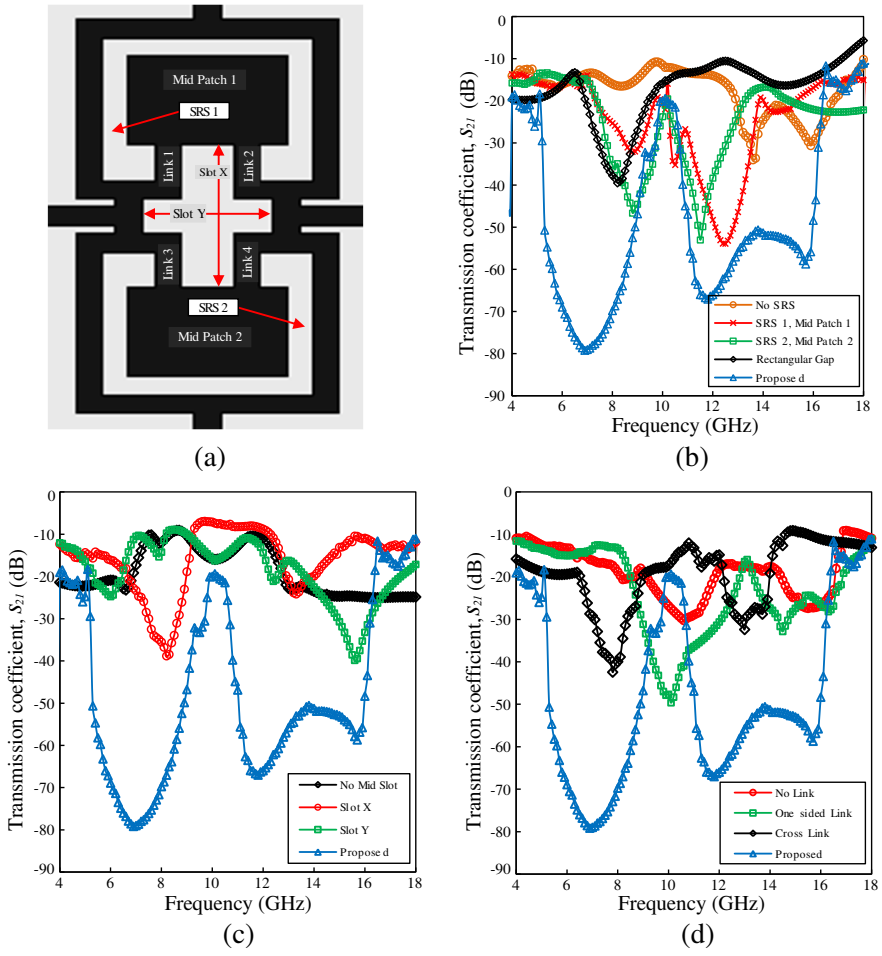

Figure 5. Determination of the dual bandgap and center frequency: (a) SRS-EBG unit; (b) Effect of the SRS and middle patch; (c) Effect of the mid slots along X and Y; (d) Effect of the connecting links.

with a connected middle patch compared to a disconnected middle patch. We investigate the cross linked cases by connecting each of the middle patches by a diagonally placed link (link 1 and 4 or link 2 and 4). In this case, the center frequencies of the bandgaps decrease to 8 GHz and 13.4 GHz, though the bandwidths are narrower than in the one-sided link case. We can conclude that these links play a very important role in determining the bandgap positions and in widening the stopband. Because both the middle patches are directly connected to the outer rings through the four links, the gap capacitance becomes balanced with the inductance to create wider bandgaps at lower frequencies than in the other cases tested.

Based on the above studies of the transmission characteristics, an array consisting of 2×3 unit cells of the proposed SRS-EBG is fabricated and measured to verify the simulated results. The design parameters are chosen as shown in Table 1.

The measured transmission spectrum of the fabricated prototype is shown in Figure 6 alongside with the simulated results for ease of comparison. The measured bandgaps are 3.65 GHz (5.2–8.85 GHz) and 4.74 GHz (10.54–15.28 GHz), and the minimum S_{21} value is around -50 dB for the two bandgaps. Both results show good agreement, though the simulated bandgaps are wider and the transmission curves (S_{21}) are deeper than in the measured results. This discrepancy may be attributed to the fabrication tolerance and the soldering of the subminiature A (SMA) connector on the two ends of the suspended line. Because the configuration is presented with optimized design parameters, the bandgaps are almost stable at 7 GHz and 13 GHz, regardless of the variation in the bandwidth and S_{21} (dB) level.

Table 1. Optimized design parameters of the proposed SRS-EBG.

Parameters	Values [mm]	Parameters	Values [mm]
a	10	k	2
b	7.5	s	1
c	2.25	t	0.5
d	1.5	W_{in}	5.5
e	3	L_{in}	3.75
f	6	W_u	12
g	5	L_u	18
h	2	W	36
i	3.5	L	36
j	1.5		

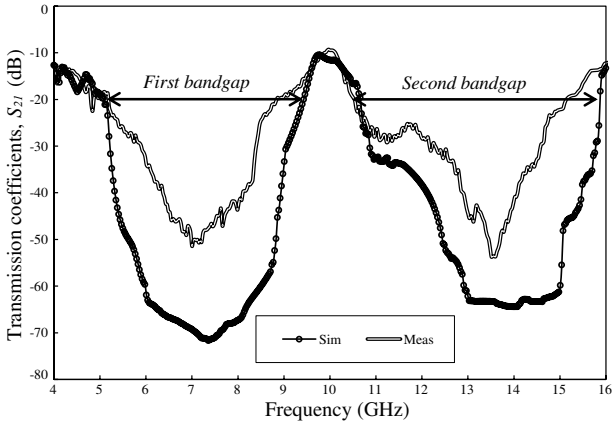

Figure 6. Comparison of simulated and measured bandgap of the SRS-EBG.

4. EBG WITH MICROSTRIP ANTENNA

The microstrip patch antennas have been used widely in communication system designs due to their numerous advantages. However, surface wave excitations degrade the antenna performance and reduce their efficiency. One of the ways to improve microstrip antenna performance is to apply an EBG structure. To investigate the effectiveness of the proposed SRS-EBG, the structure is applied to microstrip antennas. Because the EBG structure proposed in this study exhibits two wide stopbands at two different frequencies, the structure is applied for two different cases: (i) microstrip antenna single element and (ii) two element microstrip patch antenna array.

4.1. Umbrella Shape Microstrip Monopole Antenna

An umbrella shape microstrip monopole antenna is designed as shown in Figure 7(a), with a classical ground plane, and in 7(b), with an SRS-EBG ground. Usually, a rectangular microstrip patch antenna is one of the basic shapes that are commonly considered in the antenna engineering field. In comparison to the conventional rectangular patch, modified shapes such as a semi-circular umbrella type radiator are widely used for their comparatively better performance characteristics, such as wider bandwidth, lower return loss value, etc. Additionally, resonance can be obtained at lower frequencies with a comparatively smaller patch size. Because the proposed SRS-EBG exhibits a wide bandgap, the umbrella type microstrip patch is considered in this

research to verify the performance enhancement ability of the proposed EBG configuration. Moreover, the objective is to show that the structure can easily be applied to more shapes than a conventional rectangular patch.

The fabricated prototypes are shown in Figures 7(c) and (d). The antenna is targeted to operate at 7 GHz, which is within the first bandgap of the SRS-EBG (5.1–9.5 GHz), to demonstrate the aftereffect of applying the EBG. The main radiating patch is set on top of a 1.6 mm thick dielectric substrate with a relative permittivity of 4.6 and a tangent loss of 0.002. The design parameters are as follows:

$$L = W = 36\,\text{mm}, \quad L_f = 8\,\text{mm}, \quad W_f = 3\,\text{mm}, \quad r = 8\,\text{mm},$$
$$l = 5.69\,\text{mm}, \quad x = 24.5\,\text{mm}, \quad y = 18\,\text{mm}$$

Initially, the monopole is examined with a classical ground plane; in

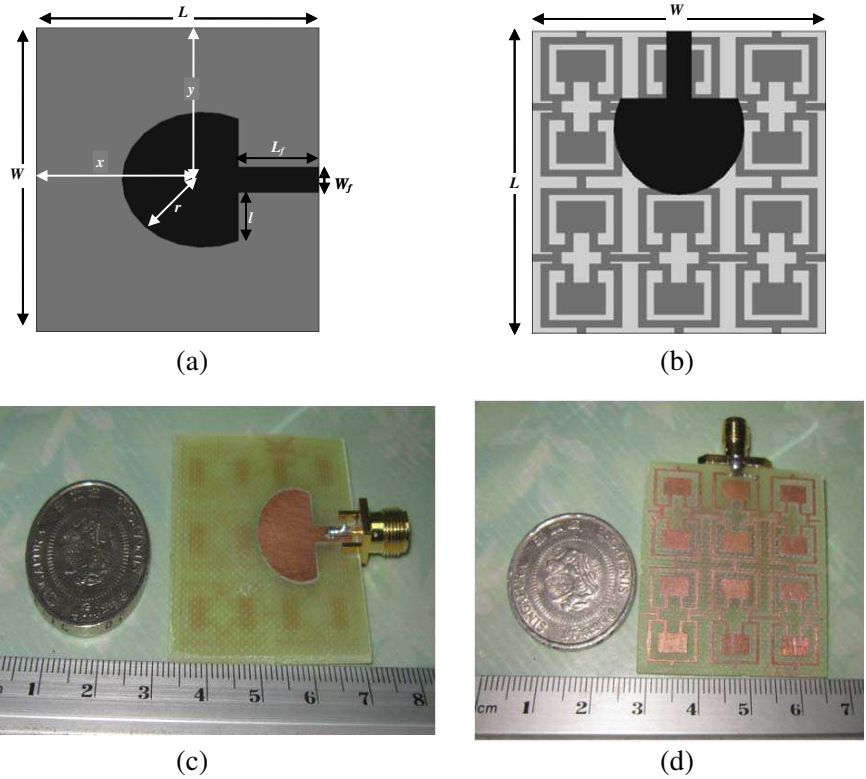

Figure 7. Microstrip monopole antenna geometry: (a) With classical ground plane; (b) With SRS-EBG; (c) Front view and; (d) Rear view of the fabricated prototypes.

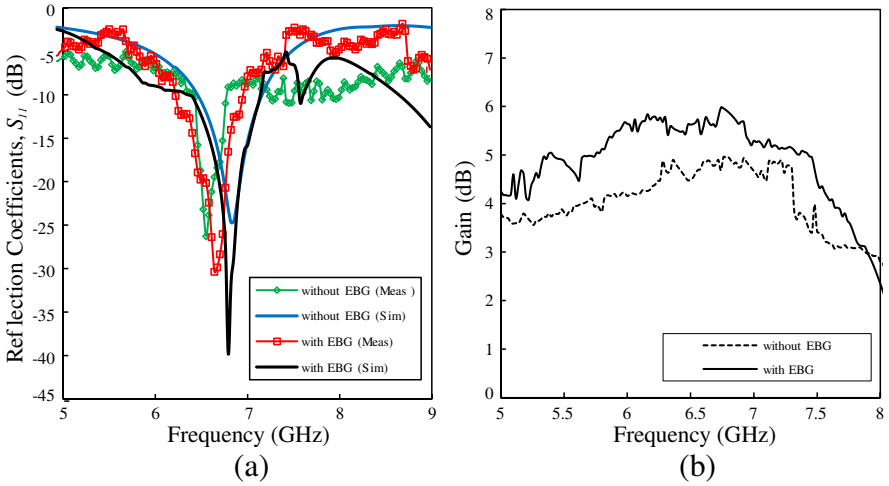

Figure 8. Comparison of simulated and measured results: (a) Reflection coefficient, S_{11}; (b) Peak gain.

later tests, the ground plane is substituted by the SRS-EBG. The in-house lab prototypes are fabricated using an LPKF ProtoMat S_{63} PCB fabrication machine. The return loss characteristics of the prototypes are measured by an Agilent's E8362C PNA network analyzer from the ANGKASA-UKM lab. The simulated and measured results are compared in Figure 8.

With a classical ground plane, the monopole resonance is approximately 6.8 GHz and exhibits a bandwidth of 0.63 GHz, covering the frequencies from 6.49 GHz to 7.12 GHz at minimum reflection coefficient of −10 dB or less. The impedance bandwidth is 9.26% with respect to the center frequency (6.76 GHz). Because the bandwidth is covered by the first bandgap (5.1–9.5 GHz) of the SRS-EBG structure, the combination of the EBG with the antenna enhances the bandwidth at a deeper reflection coefficient level (−40 dB). The EBG antenna achieves a bandwidth of 0.74 GHz, which is 11.25% with respect to the center frequency of 6.5 GHz. The measured results closely match the simulated results, despite the resonance shifting to a lower frequency. The measured minimum level of the reflection coefficient is −26 dB for the classical antenna and −31 dB for the EBG antenna. As depicted in Figure 8 (b), the peak gain achieved without the EBG is approximately 4 dB; the peak gain achieved with the EBG is greater than 5 dB. Thus, on average, more than 1 dB gain improvement is observed throughout the antenna's operating band. The simulated and measured results for both antenna cases are tabulated in Table 2.

Table 2. Microstrip monopole performance with and without SRS-EBG.

	Simulated		*Measured*	
	Without EBG	*With EBG*	*Without EBG*	*With EBG*
Resonance frequency, GHz	6.82	6.79	6.55	6.64
Minimum return loss, dB	−24.68	−40	−26.28	−30.37
Operating band, GHz	6.49–7.12	6.40–7.13	6.40–6.76	6.21–6.95
Bandwidth	9.26% (0.63 GHz)	10.8% (0.73 GHz)	5.47% (0.36 GHz)	11.25% (0.74 GHz)
Peak gain, dB	5.2	6.4	4.89	5.46

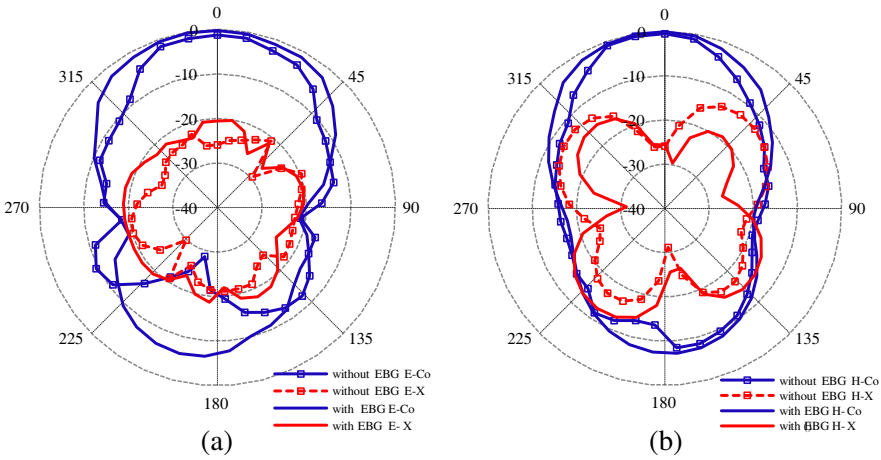

Figure 9. Normalized radiation characteristics at 6.50 GHz: (a) *E*-plane pattern; (b) *H*-plane pattern.

Figure 9 shows the normalized radiation characteristics of the monopole antenna with and without the EBG at 6.5 GHz. The EBG structure can reduce surface waves and block unwanted spurious radiation, and its application improves radiation characteristics, gain, etc.. Broadside radiation is enhanced in both the *E*- and *H*-planes, and the directivity is increased. As expected, better co-polarization level than cross-polarization is observed; the levels of cross polarization are −21 dB in the *E*-plane and −24 dB in the *H*-plane. The half power beam widths (HPBW) for the *E*- and *H*-planes are 78°and 55°, respectively. At the designed frequency, the back radiation becomes large, primarily due to the presence of the 2D slotted EBG etched in the ground plane. This effect implies that the slotted EBG can act

as slot antenna with backward radiation. In addition, the fabrication and measurement mismatch cannot be ignored. Nevertheless, the front beam broadens and the gain increases. This backward radiation level can be reduced by using a shielding plane or cavity. However, a shielding plane separated from the rear side of the antenna by a foam dielectric generates parallel plate modes and reduces antenna efficiency. A cavity can be added to enclose the antenna, but this addition can narrow the bandwidth and cause critical machining and manufacturing issues [33].

5. MUTUAL COUPLING REDUCTION OF ARRAY

The proposed dual band SRS-EBG (shown in Figure 1) is validated by applying it to a microstrip patch antenna array. In designing a compact array, size reduction can be achieved by placing the array elements close to each other, but coupling issues arise when the near-field zone of the elements overlap. A high level of coupling between array elements is introduced by surface waves. The surface waves generated have a significant effect on the antenna array, especially in the case of array elements on high permittivity substrates. Mutual coupling between array elements causes blind scanning of the array and produces an overlap of received signals. The coupling effect gradually becomes worse at higher frequencies and with increasing permittivity and substrate thickness. It has been found that E-plane coupled antennas suffer from stronger mutual coupling than H-plane coupled antennas. In comparison to the other techniques such as cavity backing or substrate removal, mutual coupling can be significantly reduced by applying EBG structures [24]. Because the EBG structure has been proven effective in reducing the coupling between array elements, an SRS-EBG is placed between a two-element array of E-plane coupled microstrip antennas, as shown in Figure 10, to check its coupling reduction ability. As described in Section 3, the proposed EBG exhibits two wide bandgaps, and the second bandgap (10–15 GHz) is considered in this case. Two identical coplanar microstrip patch antennas with a resonant frequency of 13 GHz are placed $0.8\,\lambda_0$ apart, where λ_0 is the free space wavelength. Each of the coaxial probe-fed patches has an area of $6.84 \times 5.56\,\text{mm}^2$ with an overall board size of $1.8\lambda_0 \times 2.5\lambda_0$. As shown in Figure 10, the microstrip antennas are placed over the same dielectric material (relative permittivity = 4.6, loss tangent = 0.02 and thickness = 1.6 mm) that is used to design the SRS-EBG. First, the coupling effect between the array elements is investigated without placing the EBG structures as shown in Figure 10(a). Then, 2×2 and 3×2 SRS-EBG matrixes are placed between the patch

antennas as depicted in Figure 10(b). The transmission coefficient (S_{21}) is measured to realize the coupling effect. This effect is obtained by exciting one of the antennas while other is loaded with a 50 Ω impedance.

Figure 11 shows a comparison of the mutual coupling between the E-plane coupled microstrip antennas with and without inclusion of an SRS-EBG. The antenna without an EBG shows a strong coupling level (S_{21}) of −19.06 dB between the patches, and the return loss level (S_{11}) is −19.41 dB at a resonant frequency of 13.1 GHz. The radiating

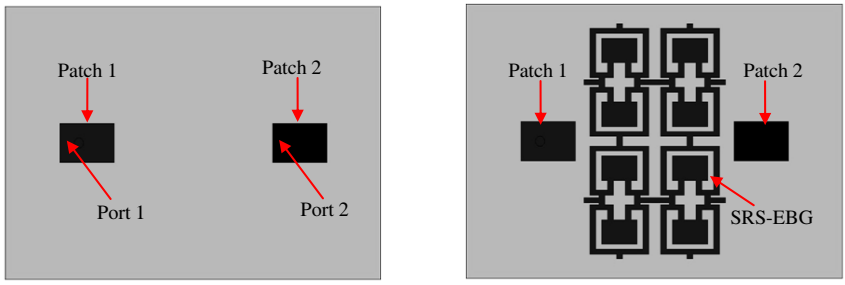

Figure 10. Two element microstrip patch antenna array: (a) Without EBG; (b) With SRS-EBG.

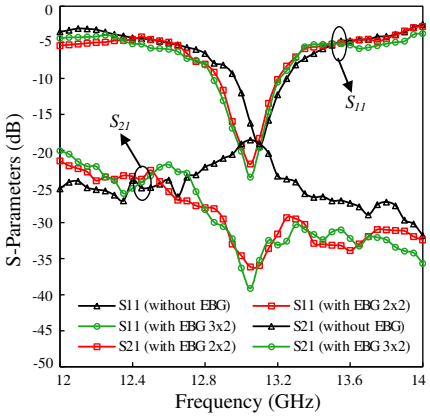

Figure 11. S-parameters of the microstrip antenna array with and without proposed EBG structure.

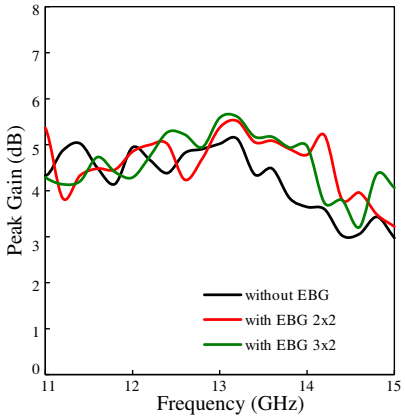

Figure 12. Peak gain of the microstrip antenna array with and without SRS-EBG.

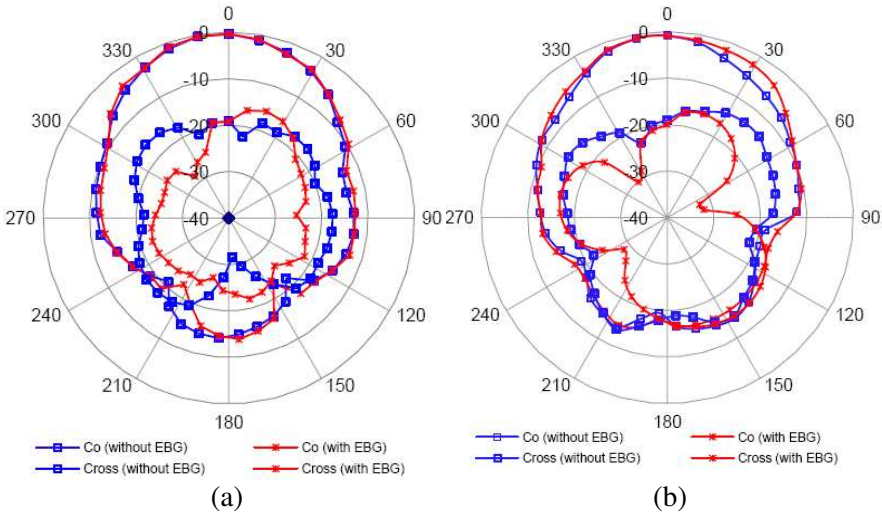

Figure 13. Normalized radiation patterns of the microstrip antenna array at 13.1 GHz with and without SRS-EBG structure: (a) E-plane patterns; (b) H-plane patterns.

patches are strongly coupled in the E-plane due to the pronounced surface waves inside the substrate. It is clear in the figure that insertion of the SRS-EBG reduces the coupling level compared to the normal case. Because the operating band of the antennas falls inside the second bandgap of the proposed SRS-EBG, the surface waves are well suppressed. The coupling level drops to -36.2 dB with a 2×2 EBG, and -39.13 dB with a 3×2 EBG. This coupling reduction by the SRS-EBG cells is mainly due to the suppression of the electric fields normal to the ground plane, which reduces the surface currents in the other antenna. Inclusion of the SRS-EBG shows that the resonances of the array shift slightly, as shown in the scattering parameters plot. However, the SRS-EBG inclusion results in deeper S_{11} levels (-21.86 dB with 2×2 EBG and -23.69 dB with 3×2 EBG) and a wider impedance bandwidth. Therefore, insertion of SRS-EBG between the antenna arrays improves the overall performance, and -20.57 dB greater reduction of the mutual coupling (S_{21}) is achieved.

The plot of peak gain versus the frequency of the array is depicted in Figure 12. The gain enhancement is nearly 0.4 dB for the 2×2 EBG array and 0.6 dB for the 3×2 EBG array. Figure 13 shows the radiation performance of the microstrip antenna array at 13.1 GHz for both E and H-planes. There is no significant effect on the main lobe

patterns from the insertion of the EBG, except for a slight increase in directivity. For both arrays, the cross-polarization level is lower than that of the co-polarization in both planes. Therefore, the addition of the SRS-EBG between microstrip arrays does not degrade the antenna efficiency or radiation characteristics; however, the main beam becomes slightly directive, in addition to reducing the mutual coupling.

6. CONCLUSION

A split-ring slotted electromagnetic bandgap (SRS-EBG) based on the uniplanar compact EBG (UC-EBG) concept is presented. The configuration possesses two wide bandgaps, despite its compactness. The bandgap behaviors of the structure are analyzed by varying different design parameters. It is shown that the bandgap and the center frequency of the bandgap can be tuned by varying some particular design parameters, while the total size remains unchanged. The proposed SRS-EBG is applied to two different cases of microstrip antennas: performance enhancement of a single antenna and mutual coupling reduction of an antenna array. Two structures are designed, fabricated, measured and compared: a microstrip antenna whose resonance falls within the first bandgap (5.11–9.40 GHz) and an array of two rectangular microstrip patch antennas whose resonance falls within the second bandgap (10.69–15.85 GHz). The single-element microstrip antenna exhibits a wider bandwidth with a deeper reflection-coefficient and 1 dB of gain enhancement with the SRS-EBG. Additionally, inclusion of the SRS-EBG in the array reduces the mutual coupling by approximately −20.57 dB and slightly improves the directivity with good co- and cross-polarization levels of the radiation patterns. The SRS-EBG is shown to be an effective and efficient way to improve the microstrip antenna performance for a single element and reduce the mutual coupling between array elements.

REFERENCES

1. Liao, W.-J., S.-H. Chang, and L.-K. Li, "A compact planar multiband antenna for integrated mobile devices," *Progress In Electromagnetics Research*, Vol. 109, 1–16, 2010.
2. Mu, X., W. Jiang, S.-X. Gong, and F.-W. Wang, "Dual-band low profile directional antenna with high impedance surface reflector," *Progress In Electromagnetics Research Letters*, Vol. 25, 67–75, 2011.
3. Xie, H.-H., Y.-C. Jiao, K. Song, and B. Yang, "Miniature electromagnetic band-gap structure using spiral ground plane,"

Progress In Electromagnetics Research Letters, Vol. 17, 163–170, 2010.

4. Tiang, J.-J., M. T. Islam, N. Misran, and J. S. Mandeep, "Circular microstrip slot antenna for dual-frequency RFID application," *Progress In Electromagnetics Research*, Vol. 120, 499–512, 2011.
5. Habib, M. A., A. Bostani, A. Djaiz, M. Nedil, M. C. E. Yagoub, and T. A. Denidni, "Ultra wideband CPW-FED aperture antenna with WLAN band rejection," *Progress In Electromagnetics Research*, Vol. 106, 17–31, 2010.
6. Gujral, M., J. L.-W. Li, T. Yuan, and C.-W. Qiu, "Bandwidth improvement of microstrip antenna array using dummy EBG pattern on feedline," *Progress In Electromagnetics Research*, Vol. 127, 79–92, 2012.
7. Abedin, M. F. and M. Ali, "Effects of a smaller unit cell planar EBG structure on the mutual coupling of a printed dipole array," *IEEE Antennas and Wireless Propagation Letter*, Vol. 4, 274–276, 2005.
8. Xie, H.-H., Y.-C. Jiao, L.-N. Chen, and F.-S. Zhang, "An effective analysis method for EBG reducing patch antenna coupling," *Progress In Electromagnetics Research Letters*, Vol. 21, 187–193, 2011.
9. Capet, N., C. Martel, J. Sokoloff, and O. Pascal, "Optimum high impedance surface configuration for mutual coupling reduction in small antenna arrays," *Progress In Electromagnetics Research B*, Vol. 32, 283–297, 2011.
10. Yang, F. and Y. Rahmat-Samii, *Electromagnetic Band-Gap Structures in Antenna Engineering*, The Cambridge RF and Microwave Engineering Series, Cambridge University Press, Cambridge, Mass, USA, 2008.
11. Wu, C.-J. and Z.-H. Wang, "Properties of defect modes in one-dimensional photonic crystals," *Progress In Electromagnetics Research*, Vol. 103, 169–184, 2010.
12. Maagt, P. D., R. Gonzalo, Y. C. Vardaxoglou, and J. M. Baracco, "Electromagnetic bandgap antennas and components for microwave and (sub)millimeter wave applications," *IEEE Transactions on Antennas and Propagation*, Vol. 51, No. 10, 2667–2777, 2003.
13. Dai, X., Y. Xiang, and S. Wen, "Broad omnidirectional reflector in the one-dimensional ternary photonic crystals containing superconductor," *Progress In Electromagnetics Research*, Vol. 120, 17–34, 2011.

14. Elsheakh, D. M. N., H. A. Elsadek, E. A.-F. Abdallah, H. M. El-Henawy, and M. F. Iskander, "Ultra-wide bandwidth microstrip monopole antenna by using electromagnetic band-gap structures," *Progress In Electromagnetics Research Letters*, Vol. 23, 109–118, 2011.
15. Xu, F., Z.-X. Wang, X. Chen, and X.-A. Wang, "Dual band-notched UWB antenna based on spiral electromagnetic-bandgap structure," *Progress In Electromagnetics Research B*, Vol. 39, 393–409, 2012.
16. Lin, M.-S., C.-H. Huang, and C.-N. Chiu, "Use of high-impedance screens for enhancing antenna performance with electromagnetic compatibility," *Progress In Electromagnetics Research*, Vol. 116, 137–157, 2011.
17. Monavar, F. M. and N. Komjani, "Bandwidth enhancement of microstrip patch antenna using jerusalem cross-shaped frequency selective surfaces by invasive weed optimization approach," *Progress In Electromagnetics Research*, Vol. 121, 103–120, 2011.
18. Kim, S.-H., T. T. Nguyen, and J.-H. Jang, "Reflection characteristics of 1-D EBG ground plane and its application to a planar dipole antenna," *Progress In Electromagnetics Research*, Vol. 120, 51–66, 2011.
19. Elsheakh, D. M. N., H. A. Elsadek, E. A.-F. Abdallah, M. F. Iskander, and H. M. El-Henawy, "Investigated new embedded shapes of electromagnetic bandgap structures and via effect for improved microstrip patch antenna performance," *Progress In Electromagnetics Research B*, Vol. 20, 91–107, 2010.
20. Liang, J. and H. Y. D. Yang, "Radiation characteristics of a microstrip patch over an electromagnetic bandgap surface," *IEEE Transactions on Antennas and Propagation*, Vol. 55, No. 6, 1691–1697, 2007.
21. Li, Y., M. Fan, F. Chen, J. She, and Z. Feng, "A novel compact electromagnetic-bandgap (EBG) structure and its applications for microwave circuits," *IEEE Transactions on Microwave Theory and Techniques*, Vol. 53, 183–190, 2005.
22. Zheng, Q.-R., B. Q. Lin, Y. Q. Fu, and N. C. Yuan, "Characteristics and applications of a novel compact spiral electromagnetic band-gap (EBG) structure," *Journal of Electromagnetic Waves and Applications*, Vol. 21, No. 2, 199–213, 2007.
23. Coccioli, R., F. R. Yang, K. P. Ma, and T. Itoh, "Aperture-coupled patch antenna on UC-PBG substrate," *IEEE Transactions on Microwave Theory and Tech.*, Vol. 47, No. 11, 2123–2130, 1999.

24. Tomeo-Reyes, I. and E. Rajo-Iglesias, "Comparative study on different HIS as ground planes and its application to low profile wire antennas design," *Progress In Electromagnetics Research*, Vol. 115, 55–77, 2011.
25. Liu, J., W.-Y. Yin, and S. He, "A new defected ground structure and its application for miniaturized switchable antenna," *Progress In Electromagnetics Research*, Vol. 107, 115–128, 2010.
26. Wang, X., M. Zhang, and S.-J. Wang, "Practicability analysis and application of PBG structures on cylindrical conformal microstrip antenna and array," *Progress In Electromagnetics Research*, Vol. 115, 495–507, 2011.
27. Abedin, M. F., M. Z. Azad, and M. Ali, "Wideband smaller unit-cell planar EBG structures and their application," *IEEE Antennas Wireless Propagation Letter*, Vol. 56, 274–276, 2008.
28. Gonzalo, R., I. Ederra, C. Mann, and P. de Maagt, "Radiation properties of terahertz dipole antenna mounted on photonic crystal," *Electronics Letters*, Vol. 37, No. 10, 613–614, 2001.
29. Yang, F. and Y. Rahmat-Samii, "Microstrip antennas integrated with electromagnetic band-gap (EBG) structures: A low mutual coupling design for array applications," *IEEE Transactions on Antennas Propag.*, Vol. 51, 2939–2949, 2003.
30. Yamamoto, M., T. Koyanagi, and T. Nojima, "Leaf-shaped bowtie antenna backed by a periodic patch-loaded grounded slab," *IEEE International Symposium on Antennas and Propagation (APSURSI)*, 622–625, 2011.
31. Assimonis, S. D., T. V. Yioultsis, and C. S. Antonopoulos, "Computational investigation and design of planar EBG structures for coupling reduction in antenna applications," *IEEE Transactions on Magnetics*, Vol. 48, No. 2, 771–774, 2012.
32. Fan, M. Y., R. Hu, Z. H. Feng, X. X. Zhang, and Q. Hao, "Advance in 2D-EBG research," *Journal of Infrared Millimeter Waves*, Vol. 22, No. 2, 2003.
33. Yin, X., H. Zhang, X.-Y. Huang, and H.-Y. Xu, "Spurious modes reduction in a patch antenna using an EBG-based microstrip transmission line filter," *Progress In Electromagnetics Research C*, Vol. 25, 41–54, 2012.